"Dip-Pen" Nanolithography
Richard D. Piner, *et al.*
Science **283**, 661 (1999);
DOI: 10.1126/science.283.5402.661

remove unreacted DSP, then lysed in RIPA buffer (*10*) before immunoprecipitation.

38. Immunoprecipitation and immunoblotting of Flag and HA epitope–tagged β_2ARs, HA epitope–tagged AT1A receptors, Flag epitope–tagged β-arrestins, and c-Src were performed with commercially available antisera as described (*9, 31*). Immunoprecipitation and immunoblotting of His^6-tagged β-arrestin 1 were performed with a rabbit polyclonal antiserum raised against a GST–β-arrestin 1 COOH-terminus fusion protein (*32*). Immune complexes on nitrocellulose were visualized by enzyme-linked chemiluminescence and quantified by scanning laser densitometry. The stoichiometry of β-arrestin 1 to c-Src in receptor immunoprecipitates was determined by normalizing immunoblot intensities to the signal obtained from known amounts of purified recombinant His^6-tagged β-arrestin 1 and c-Src resolved along with the receptor immunoprecipitates.
39. Flag epitope–tagged truncation or deletion mutants of β-arrestin 1 were prepared by the polymerase chain reaction (PCR), incorporating an Eco RI site, minimal Kozak sequence (ACC), and initiator methionine codon into the 5′ primer, and the Flag epitope sequence, stop codon, and an Xho I site into the 3′ primer. PCR products were subcloned into a peptide minigene expression cassette as described (*33*). DNA sequences were confirmed by dideoxynucleotide sequencing.
40. Recombinant His^6-tagged β-arrestin 1 and recombinant human c-Src or c-Src SH2 or SH3 domain GST fusion proteins were combined for 20 min at room temperature in 20 μl of 10 mM Pipes (pH 7.0) before samples were diluted with 0.5 ml RIPA buffer, and His^6-tagged β-arrestin 1 was immunoprecipitated using rabbit polyclonal anti-His^6 immunoglobulin G (IgG). After resolution by SDS-PAGE, both the His^6-tagged β-arrestin 1 and coprecipitated Src-GST fusion proteins were detected simultaneously by protein immunoblotting with rabbit polyclonal anti-GST–β-arrestin 1. Competition for binding between c-Src and GST–Src SH2 or GST–Src SH3 was performed with the GST-Src fusion protein in 20-fold excess.
41. 12CA5 epitope–tagged β_2ARs (500 to 1000 fmol/mg whole-cell protein) expressed in HEK-293 cells in six-well plates were treated with or without isoproterenol for 30 min in serum-free medium at 37°C. Cell surface receptors were labeled with 12CA5 mAb, using fluorescein isothiocyanate–conjugated goat antibody to mouse IgG as secondary antibody. Receptor sequestration was quantified as loss of cell surface receptors, as measured by flow cytometry (*34*). Receptor expression was determined by saturation binding of [^{125}I]pindolol.
42. Aliquots of whole-cell lysate from appropriately stimulated cells (30 μg of protein per lane) were resolved by SDS-PAGE, and Erk 1 and Erk2 phosphorylation was detected by protein immunoblotting with rabbit polyclonal phospho-MAP kinase–specific IgG. Quantitation of Erk 1 and Erk2 phosphorylation was performed with a Storm Phosphorimager. After quantitation of Erk 1 and Erk2 phosphorylation, nitrocellulose membranes were stripped of Ig and reprobed with rabbit polyclonal anti-Erk 2 IgG to confirm equal loading of Erk protein.
43. R.J.L. and M.G.C. are investigators with the Howard Hughes Medical Institute. Supported in part by NIH grants DK02352 and DK55524 (L.M.L), HL16037 (R.J.L), NS19576 (M.G.C.), and Heart and Stroke Foundation of Ontario Grant NA3349 (S.S.G.F.). G.J.D.R. is supported by NIH Medical Scientist Training Program Grant T32GM-07171. We thank M. J. Eck for purified recombinant c-Src and D. Addison and M. Holben for excellent secretarial assistance.

27 May 1998; accepted 17 November 1998

REPORTS

"Dip-Pen" Nanolithography

Richard D. Piner, Jin Zhu, Feng Xu, Seunghun Hong, Chad A. Mirkin*

A direct-write "dip-pen" nanolithography (DPN) has been developed to deliver collections of molecules in a positive printing mode. An atomic force microscope (AFM) tip is used to write alkanethiols with 30-nanometer linewidth resolution on a gold thin film in a manner analogous to that of a dip pen. Molecules are delivered from the AFM tip to a solid substrate of interest via capillary transport, making DPN a potentially useful tool for creating and functionalizing nanoscale devices.

Lithographic methods are at the heart of modern-day microfabrication, nanotechnology, and molecular electronics. These methods often rely on patterning of a resistive film, followed by a chemical etch of the substrate. Dip-pen technology, in which ink on a sharp object is transported to a paper substrate via capillary forces, is approximately 4000 years old (*1*) and has been used extensively throughout history to transport molecules on macroscale dimensions. Here we report experiments that merge these two related but, with regard to scale and transport mechanism, disparate concepts to develop a new type of dip-pen nanolithography (DPN). DPN uses an atomic force microscope (AFM) tip as a "nib," a solid-state substrate (in this case, Au) as "paper," and molecules with a chemical affinity for the solid-state substrate as "ink." Capillary transport of molecules from the AFM tip to the solid substrate is used in DPN to directly "write" patterns consisting of a relatively small collection of molecules in submicrometer dimensions.

DPN is not the only lithographic method that allows one to directly transport molecules to substrates of interest in a positive printing mode. For example, microcontact printing, which uses an elastomer stamp, can deposit patterns of thiol-functionalized molecules directly onto Au substrates (*2–6*). This method is a parallel technique, allowing one to deposit an entire pattern or series of patterns on a substrate of interest in one step (*2–19*), which is an advantage over a serial technique such as DPN unless one is trying to selectively place different types of molecules at specific sites within a particular type of nanostructure. In this regard, DPN complements microcontact printing and many other existing methods of micro- and nanofabrication (*2–19*). Finally, there are a variety of negative printing techniques that rely on scanning probe instruments, electron beams, or molecular beams to pattern substrates, using self-assembled monolayers (SAMs) and other organic materials as resist layers (*7–19*), that is, to remove material for subsequent processing or adsorption steps. However, DPN can deliver relatively small amounts of a molecular substance to a substrate in a nanolithographic fashion that does not rely on a resist, a stamp, complicated processing methods, or sophisti-

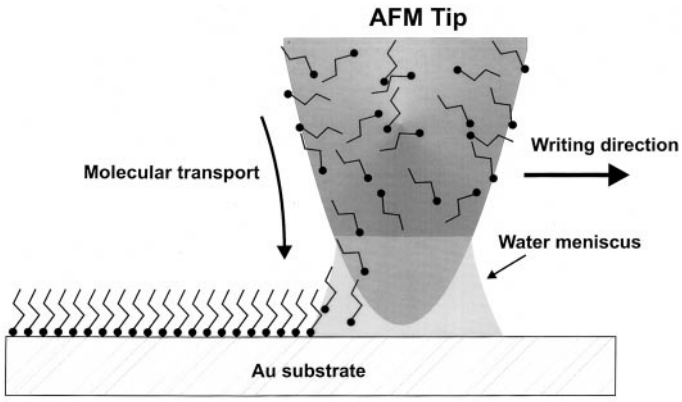

Fig. 1. Schematic representation of DPN. A water meniscus forms between the AFM tip coated with ODT and the Au substrate. The size of the meniscus, which is controlled by relative humidity, affects the ODT transport rate, the effective tip-substrate contact area, and DPN resolution.

Department of Chemistry, Northwestern University, 2145 Sheridan Road, Evanston, IL 60208, USA.

*To whom correspondence should be addressed. E-mail: camirkin@chem.nwu.edu

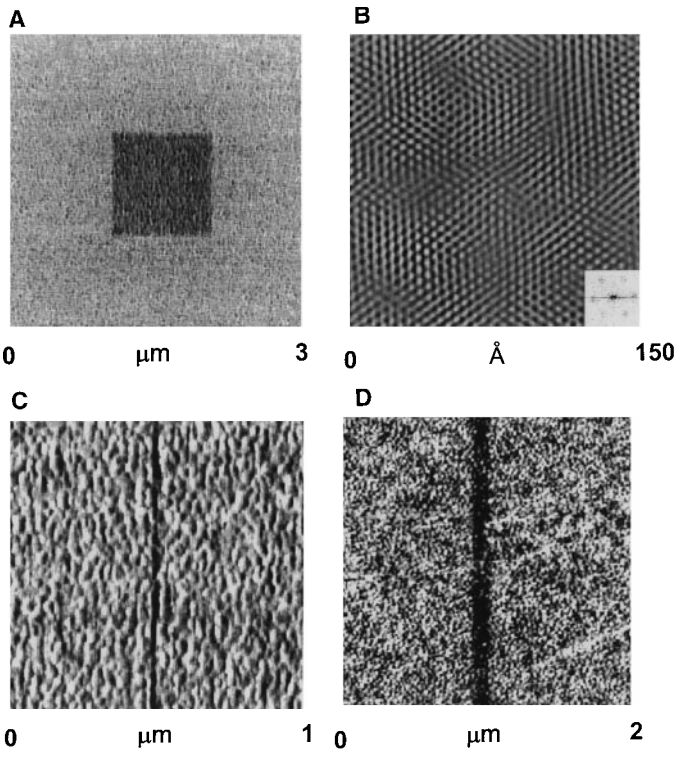

Fig. 2. (**A**) Lateral force image of a square of ODT measuring 1 μm by 1 μm, deposited onto a Au substrate by DPN. This pattern was generated by scanning the 1-μm^2 area at a scan rate of 1 Hz for a period of 10 min at a relative humidity of 39%. Then the scan size was increased to 3 μm, and the scan rate was increased to 4 Hz while the image was recorded. The faster scan rate prevents ODT transport. (**B**) Lattice-resolved, lateral force image of an ODT SAM deposited onto Au(111)/mica by DPN. The image has been filtered with a fast Fourier transform (FFT), and the FFT of the raw data is shown in the lower right insert. The monolayer was generated by scanning a 1000 Å square area of the Au(111)/mica five times at a rate of 9 Hz at 39% relative humidity. (**C**) Lateral force image of a 30-nm-wide line (3 μm long) deposited onto Au/mica by DPN. The line was generated by scanning the tip in a vertical line repeatedly for 5 min at a scan rate of 1 Hz. (**D**) Lateral force image of a 100-nm line deposited on Au by DPN. The method of depositing this line is analogous to that used to generate the image in (C), but the writing time was 1.5 min. In all images, darker regions correspond to areas of relatively lower friction.

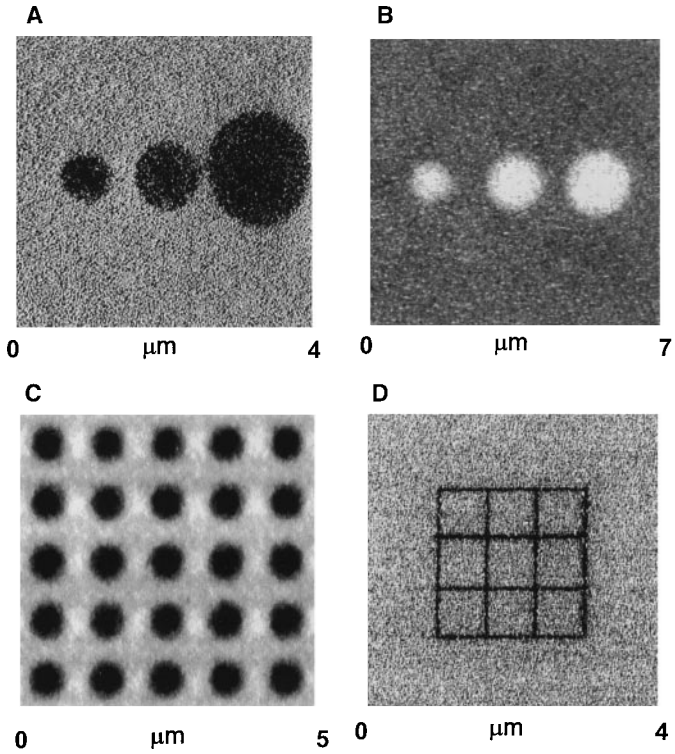

Fig. 3. (**A**) Lateral force image of an Au substrate after an AFM tip, which was coated with ODT, had been in contact with the substrate for 2, 4, and 16 min (left to right); the relative humidity was held constant at 45%, and the image was recorded at a scan rate of 4 Hz. (**B**) Lateral force image of dots of 16-mercaptohexadecanoic acid on a Au substrate. To generate the dots, an AFM tip coated with 16-mercaptohexadecanoic acid was held on the Au substrate for 10, 20, and 40 s (left to right). The relative humidity was 35%. The images show that the transport properties of 16-mercaptohexadecanoic acid and of ODT differ substantially. (**C**) Lateral force image of an array of dots generated by DPN. Each dot was generated by holding an ODT-coated tip in contact with the surface for ~20 s. Writing and recording conditions were the same as in (A). (**D**) Lateral force image of a molecule-based grid. Each line is 100 nm in width and 2 μm in length and required 1.5 min to write.

cated noncommercial instrumentation.

The inspiration for this methodology came from the study of a problem that has plagued the AFM since its invention. The narrow gap capillary formed between the AFM tip and the sample when an experiment is conducted in air (*20–23*) condenses water from the ambient and substantially influences imaging experiments especially those attempting to achieve nanometer or even angstrom resolution (*20–23*). In our own work (*23*), we have shown that this is a dynamic problem and that water, depending on relative humidity and substrate wetting properties, will either be transported from the substrate to the tip or vice versa. In the latter case, metastable nanometer-length–scale patterns could be formed from very thin layers of water deposited from the AFM tip (*23*). We now show that when the transported molecules can anchor themselves to the substrate through chemisorption, stable surface structures are formed, resulting in a new type of nanolithography, DPN (Fig. 1).

Although we have investigated the transport process with several molecules, we focus on the transfer of 1-octadecanethiol (ODT) to Au surfaces, a system that has been studied extensively (*24–28*). This moderately air-stable molecule, when immobilized on Au, can be easily differentiated from unmodified Au by means of lateral force microscopy (LFM). Our studies suggest that when an AFM tip coated with ODT is brought into contact with a sample surface, the ODT flows from the tip to the sample by capillary action, a process much like that of a dip pen (Fig. 1). We have studied this process using a conventional AFM (*29*) on thin film substrates that were prepared by thermally evaporating 300 Å of polycrystalline Au onto mica at room temperature. For these experiments, a silicon nitride tip (Park Scientific, Microlever A) was coated with ODT by dipping of the cantilever into a saturated solution of ODT in acetonitrile for 1 min. The cantilever was blown dry with compressed difluoroethane before being used. A simple demonstration of this process involves raster scanning of a tip that was prepared in this manner across a section of a Au substrate measuring 1 μm by 1 μm (Fig. 2A). An LFM image of this section within a larger scan area (3 μm by 3 μm) shows two areas of differing contrast. The interior dark area, or region of lower lateral force, is a deposited monolayer of ODT, and the exterior lighter area is bare Au (*22*). Formation of high-quality SAMs occurs when the deposition process is carried out on Au(111)/mica, which was prepared by annealing our Au thin film substrates at 300°C for 3 hours (*28*). In this case, it was possible to obtain a lattice-resolved image of an ODT SAM (Fig. 2B). The hexagonal lattice parameter of 5.0 ± 0.2 Å compares well with reported values for SAMs of ODT on Au(111) (*28*) and shows that ODT, rather than some other adsorbates (water or acetonitrile),

are transported from the tip to the substrate. Although the experiments performed on Au(111)/mica provide important information about the chemical identity of the transported species in these experiments, Au(111)/mica is a poor substrate for DPN. The deep valleys around the small Au(111) facets make it difficult to draw long (micrometer) contiguous lines with nanometer widths.

Although the nonannealed Au substrates are relatively rough (the root mean square roughness is 2 nm), we could deposit 30-nm lines with DPN; this distance is the average Au grain diameter of our thin film substrates and represents the resolution limit of DPN on this type of substrate (Fig. 2C). The 30-nm molecule-based line prepared on this type of substrate is discontinuous and follows the grain edges of the Au. Smoother and more contiguous lines can be drawn by increasing the line width to 100 nm (Fig. 2D) or presumably by using a smoother Au substrate. The width of the line depends on tip scan speed and the rate of transport of the alkanethiol from the tip to the substrate (relative humidity can change the transport rate). Faster scan speeds and a smaller number of traces give narrower lines.

We also used DPN to prepare molecular dot features to demonstrate the diffusion properties of the "ink" (Fig. 3, A and B). The ODT-coated tip was brought into contact (set point = 1 nN) with the Au substrate for a set period of time. For example, ODT dots 0.66 μm, 0.88 μm, and 1.6 μm in diameter were generated by holding the tip in contact with the surface for 2, 4, and 16 min, respectively (Fig. 3A, left to right). The uniform appearance of the dots probably reflects an even flow of ODT in all directions from the tip to the surface. Opposite contrast images were obtained by depositing dots of an alkanethiol derivative, 16-mercaptohexadecanoic acid, in an analogous fashion (Fig. 3B). This not only provides additional evidence that the molecules are being transported from the tip to the surface but also demonstrates the molecular generality of DPN.

We could generate arrays and grids in addition to individual lines and dots. An array of 25 ODT dots 0.46 μm in diameter, spaced 0.54 μm apart (Fig. 3C), was generated by holding an ODT-coated tip in contact with the surface (1 nN) for 20 s at 45% relative humidity without lateral movement to form each dot. A grid consisting of eight intersecting lines 2 μm in length and 100 nm wide (Fig. 3D) was generated by sweeping the ODT-coated tip on a Au surface at a 4-μm/s scan speed with a 1-nN force for 1.5 min to form each line.

The resolution of DPN depends on several parameters, and its ultimate resolution is not yet clear. First, the grain size of the substrate affects DPN resolution much as the texture of paper controls the resolution of conventional writing. Second, chemisorption and self assembly can be used to limit the diffusion of the molecules after deposition. The ODT patterns are stable whereas water forms metastable patterns (*23*). Third, the tip-substrate contact time and thus the scan speed influence DPN resolution. Fourth, relative humidity seems to affect the resolution of the lithographic process by controlling the rate of ODT transport from the tip to the substrate. The size of the water meniscus that bridges the tip and substrate depends on relative humidity (*23*). For example, the 30-nm-wide line (Fig. 1C) required 5 min to generate in a 34% relative humidity environment, whereas the 100-nm line (Fig. 1D) required 1.5 min to generate in a 42% relative humidity environment.

DPN is a simple but powerful method for transporting molecules from AFM tips to substrates at resolutions comparable to those achieved with much more expensive and sophisticated competitive lithographic methods, such as electron-beam lithography. It should be especially useful for the detailed functionalization of nanoscale devices prepared by more conventional lithographic methods (*30*, *31*).

References and Notes

1. A. C. Ewing, *The Fountain Pen: A Collector's Companion* (Running Press, Philadelphia, PA, 1997).
2. Y. Xia and G. M. Whitesides, *Angew. Chem. Int. Ed. Engl.* **37**, 550 (1998).
3. E. Kim, Y. Xia, G. M. Whitesides, *Nature* **376**, 581 (1995).
4. Y. Xia *et al.*, *Science* **273**, 347 (1996).
5. L. Yan, X.-M. Zhao, G. M. Whitesides, *J. Am. Chem. Soc.* **120**, 6179 (1998).
6. A. Kumar, H. A. Biebuyck, N. L. Abbott, G. M. Whitesides, *ibid.* **114**, 9188 (1992).
7. L. A. Bottomley, *Anal. Chem.* **70**, 425R (1998).
8. R. M. Nyffenegger and R. M. Penner, *Chem. Rev.* **97**, 1195 (1997).
9. K. K. Berggren *et al.*, *Science* **269**, 1255 (1995).
10. J. A. M. Sondag-Huethorst, H. R. J. van Helleputte, L. G. J. Fokkink, *Appl. Phys. Lett.* **64**, 285 (1994).
11. J. K. Schoer and R. M. Crooks, *Langmuir* **13**, 2323 (1997).
12. S. Xu and G. Liu, *ibid.*, p. 127.
13. F. K. Perkins *et al.*, *Appl. Phys. Lett.* **68**, 550 (1996).
14. D. W. Carr *et al.*, *J. Vac. Sci. Technol. A* **15**, 1446 (1997).
15. M. J. Lercel, H. G. Craighead, A. N. Parikh, K. Seshadri, D. L. Allara, *Appl. Phys. Lett.* **68**, 1504 (1996).
16. H. Sugimura and N. Nakagiri, *J. Vac. Sci. Technol. A* **14**, 1223 (1996).
17. T. Komeda, K. Namba, Y. Nishioka, *ibid.* **16**, 1680 (1998).
18. H. U. Muller, C. David, B. Volkel, M. Grunze, *J. Vac. Sci. Technol. B* **13**, 2846 (1995).
19. Y. Kim and C. M. Lieber, *Science* **257**, 375 (1992).
20. L. Xu, A. Lio, J. Hu, D. F. Ogletree, M. Salmeron, *J. Phys. Chem. B* **102**, 540 (1998).
21. M. Binggeli and C. M. Mate, *Appl. Phys. Lett* **65**, 415 (1994).
22. M. Fujihira *et al.*, *Chem. Lett.* (1996), p. 499.
23. R. D. Piner and C. A. Mirkin, *Langmuir* **13**, 6864 (1997).
24. C. D. Bain and G. M. Whitesides, *Angew. Chem. Int. Ed. Engl.* **28**, 506 (1989).
25. A. Ulman, *An Introduction to Ultrathin Organic Films: From Langmuir-Blodgett to Self-Assembly* (Academic Press, Boston, MA, 1991).
26. L. H. Dubois and R. G. Nuzzo, *Annu. Rev. Phys. Chem.* **43**, 437 (1992).
27. A. R. Bishop and R. G. Nuzzo, *Curr. Opin. Coll. Interf. Sci.* **1**, 127 (1996).
28. C. A. Alves, E. L. Smith, M. D. Porter, *J. Am. Chem. Soc.* **114**, 1222 (1992).
29. A Park Scientific Model CP instrument was used to perform all experiments. The scanner was enclosed in a glass isolation chamber, and the relative humidity was measured with a hygrometer. All humidity measurements have an absolute error of ±5%.
30. M. A. Reed, C. Zhou, C. J. Muller, T. P. Burgin, J. M. Tour, *Science* **278**, 252 (1997).
31. D. L. Feldheim and C. D. Keating, *Chem. Soc. Rev.* **27**, 1 (1998).

32. C.A.M. acknowledges the Air Force Office of Scientific Research and the NSF-funded Northwestern University Materials Research Center for support of this work.

24 September 1998; accepted 22 December 1998

Visible Quantum Cutting in $LiGdF_4:Eu^{3+}$ Through Downconversion

René T. Wegh, Harry Donker, Koenraad D. Oskam, Andries Meijerink*

For mercury-free fluorescent lamps and plasma display panels, alternative luminescent materials are required for the efficient conversion of vacuum ultraviolet radiation to visible light. Quantum cutting involving the emission of two visible photons for each vacuum ultraviolet photon absorbed is demonstrated in Eu^{3+}-doped $LiGdF_4$ with the concept of downconversion. Upon excitation of Gd^{3+} with a high-energy photon, two visible photons can be emitted by Eu^{3+} through an efficient two-step energy transfer from Gd^{3+} to Eu^{3+}, with a quantum efficiency that approaches 200 percent.

Luminescent materials with lanthanides are found in fluorescent tubes, color televisions, x-ray photography, lasers, infrared (IR) to visible light upconversion materials, and fiber amplifiers (*1*–*3*). Such applications rely on the luminescence properties of lanthanide ions (sharp lines and high efficiency). In fluorescent lamps, phosphors on the inside wall of the glass tube convert the ultraviolet (UV) radiation (mainly with a wavelength λ of 254